# Plasma Discharge Ionization Emission Spectra of Analytes and SARS-CoV-2 for Label-Free Sensing Applications

Massood Tabib-Azar, *Senior Member, IEEE*, and Braden Aaron Brown

***Abstract*—Ionization spectra of substances are extensively used in their label free detection. Here we demonstrate the possibility of using plasma ionization to detect airborne and saliva SARS-COV-2 viruses through their emission spectra. It consists of an ionization chamber monitored by a fiber-optic UV-VIS spectrometer. The technique is completely label-free and can be programmed in real-time to detect different viral particles through their ionization emission spectra. Its average sensitivity for detecting deoxyribonucleic acid (DNA) bases in water is 20%/g in 1 mL of water. Its selectivity for DNA bases is through their relative emission peaks for adenine at 439.5 nm, cytosine at 440, thymine at 440.5, and guanine at 421.5 nm. The emission spectra of different electrode materials were also obtained to account for their contributions to the emission spectra of analytes. Gold electrodes were used owing to their resistance to corrosion and very low reaction with ionized species. The technique has the potential to be used in the point-of-care diagnostic and testing applications.**

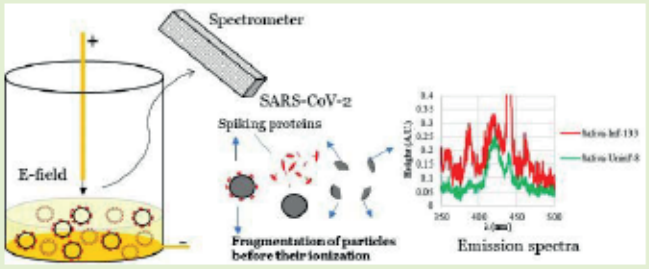


***Index Terms*— Label-free sensing, programmable sensors, ionization sensors.**

## I. Introduction

LABEL-FREE free detection of viral particles, especially in the airborne phase can be potentially a game changer in monitoring the spread of respiratory infectious diseases and harmful particles such as asbestos. Identification of metals through their emission spectra has been known and practiced since the 19th century [1], [2], [3] and flame ionization spectroscopy has also been used in gas chromatography for a long time [4]. Prehistoric humans likely noticed different colors of light emitted in a pit fire from different trees and shrubs or burning of different animal tissues.

Application of ionization spectroscopy to identify extended objects such as viral particles is not well-established, however. Here we demonstrate the ability of the plasma ionization in detecting different salts dissolved in water, uninfected saliva and SARS-CoV-2 infected saliva.

Fig. 1 schematically shows different ionization spectroscopies. A source of ionization, that can take many different forms, is used to ionize molecules or particles near a liquid surface that can be electrophoretically moved to the liquid surface before ionization. Alternatively, ultrasonication or a nebulizer can be used to produce a spray of the liquid and its content into an ionization chamber. The ionization process can be initiated by many different techniques such as x-rays [5], UV [6], electron beams [7], large DC fields [8], and flame [9]. The main difference between these different ionization techniques is their ability to control the ionization process. The DC plasma generation and flame ionization techniques, for examples, have the least control while UV, X-ray, electron beam, laser, and RF/microwave (capacitive and inductive) plasma ionization techniques can be used to exquisitely control the

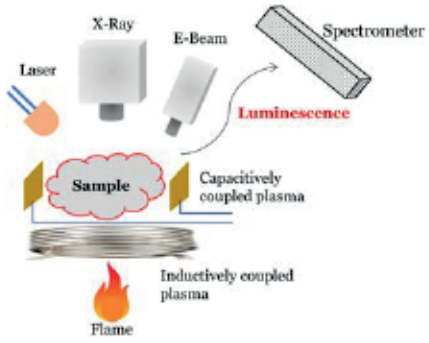


Fig. 1. Different mechanisms can be used to ionize materials. Not all possible excitation sources are shown.

Manuscript received November 21, 2021; revised January 20, 2022; accepted January 23, 2022. Date of publication February 1, 2022; date of current version March 14, 2022. This work was supported in part by the NSF under RAPID Grant 2030359, in part by EXAMIN, in part by LLC, and in part by the Utah Science Technology and Research Initiative (USTAR) Program. The associate editor coordinating the review of this article and approving it for publication was Dr. Shyqyri Haxha. *(Corresponding author: Massood Tabib-Azar.)*

The authors are with the Electrical and Computer Engineering Department, The University of Utah, Salt Lake City, UT 84112 USA (e-mail: azar.m@utah.edu; u1013992@utah.edu).

Digital Object Identifier 10.1109/JSEN.2022.3146845

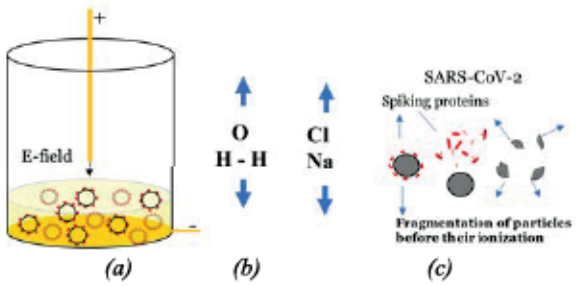


Fig. 2. a) Sample vial with gold electrodes. b) Water molecules and ionic species can be ionized with sufficiently large electric fields. c) Viral and other larger particles may be dissociated and fragmented before ionization of their constituents. SARS-CoV-2 may lose its spiking proteins before decomposing to its RNA and surface proteins that will be subsequently ionized.

ionization process through atomic/molecular quantum energy levels [10]. In our experiments reported here, we used DC plasma ionization process along with a UV-VIS fiber optics spectrometer, (Ocean Optics ST2000) with 0.1 nm wavelength resolution.

Here we discuss the DC plasma ionization spectra of aqueous solutions of different salts and saliva with and without SARS-CoV-2 viral infection. The technique is label-free and self-cleaning/sanitizing.

## II. Rationale and Theoretical Foundation

Excitation and ionization of materials may lead to oxidation/reduction reactions with nearby substances and gases (molecules). In the case of viral and other extended particles, the excitation process may have many different stages involving 1) evaporation of their surface moisture, 2) decomposition of their surface proteins, or in the case of SARS-CoV-2 detachments of its spiking proteins, 3) decomposition of their internal macro-molecules such as DNA or RNA, and finally, 4) ionization of these different components [11]. At some of these ionization and dissociation stages, there may be luminescence that can be detected to identify the excitation and decomposition process.

Fig. 2 schematically shows the electrodes and a liquid sample holder we have developed to carry out experiments reported here. Large voltages (1000-5000 V) are applied between the top and bottom electrodes (separation ~2-3 mm) and the molecules on the liquid surface are exposed to large polarizing fields. If these fields become sufficiently large ($\sim 10^4$-$10^5$ V/cm), the liquid surface molecules can be ionized. The interaction causing ionization is based on formation of electric dipoles and polarization of the molecules in the presence of large electric fields. In addition to molecular polarizations, charging of molecules can also occur by direct tunneling of charges from electrodes or by ion-assisted field enhancement. There are extensive data bases that list ionization energies/potentials of different substances. The actual voltages required to ionize substances in a device depends on many different parameters that are extensively studied in the context of gas lasers and plasmas. In aqueous solutions, water molecules dominate with H-O bond energy of 5.15 eV. Under intense electric field water evaporates and increases the effective dielectric constant of the air. Other ions in the solution such as $Na^+$ and $Cl^-$ can also be ionized and detected through their light emission. Larger molecules involving proteins, DNA and other macromolecules will be subject to electrostatic forces and may wander close enough to the liquid surface to be subject to strong dissociating and ionizing fields. In the case of SARS-COV-2 schematically shown in Fig. 2c, the dissociation may occur in the form of detaching its spiking proteins followed by its fragmentation. Most of the bonds in these excitations are covalent bonds between carbon, hydrogen, and oxygen atoms.

Electric dipole interaction is the primary mechanism of field ionization of molecules and fragmentation of particles, other extended particles, and their subsequent ionization. While polar molecules readily orient themselves with the external electric field through electric dipole interactions, non-polar molecules become polarized first by the fast response of their electronic orbitals. Particles and extended objects also acquire residual charges (or tunneling charges from nearby electrodes) and polarization before fragmentation and then ionization.

Field ionization can also be used to detect airborne viral and other particles [12]. The density of airborne particles is lower than in the liquid phase, necessitating the utilization of concentrators and photomultipliers in detecting the electroluminescent/fluorescent emission spectra.

Here we discuss an atmospheric DC plasma technique [9] with the goal of developing a label-free technique for detecting viral particles using the ST2000 Oceanview UV-VIS fiber-optic spectrometer. Fig. 1 shows the schematic of the experimental setup.

In section II we discussed the theoretical foundation of the plasma discharge ionization process with solid-liquid electrodes. In section III we describe and discuss the experimental results. In section IV we discuss miniaturization of the proposed sensing system followed by the conclusion in section V.

## III. Experimental Results and Discussion

Plasma ionization of atoms, molecules and macro-molecules have been used extensively to identify metals [1], and to detect and quantify sulfur in petroleum [10]. We are extending these techniques to detect viral particles in saliva and potentially in sewage water.

To accomplish this, our experiments made use of a vial with gold electrodes as shown in Fig. 2, an ST2000 Ocean optics fiber optic spectrometer, and a BK Precision DC regulated power supply. For each liquid solution being analyzed, 30 $\mu$L of the liquid was injected on top of the bottom electrode. A cap containing the top electrode was then placed on top of the vial to contain liquid and gaseous products of the ionization process. The DC power supply, which was connected to an amplifier, was then slowly turned on and increased in power until plasma became visible. A cardboard box was placed on top of set up to block out extra light that could be picked up by the fiber optic spectrometer as noise. Data was collected using an OceanView application that reported the intensity level at

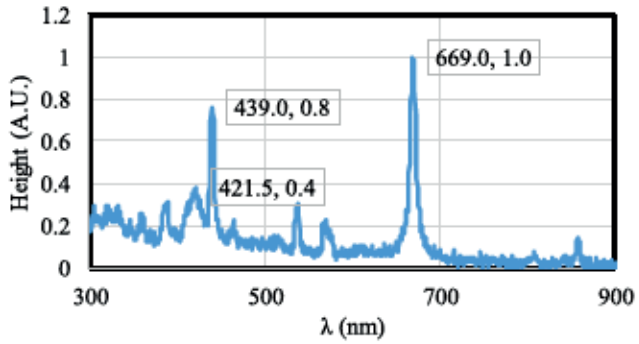


Fig. 3. Normalized plot of emission-spectra of gold electrodes.

TABLE I
TABULATED RESULTS OF EMISSION SPECTRA PEAKS OF DIFFERENT ELECTRODE MATERIALS

| Electrode | 1st Peak λ* | 2nd Peak λ* | 3rd Peak λ* |
|---|---|---|---|
| Au-Au | 669.0 | 439.0 | 421.5 |
| Cu-Cu | 668.5 | 439.5 | 418.5 |
| Fe-Fe | 440.5 | 387 | 537 |
| Au-Cu | 668.5 | 439.5 | 418.5 |
| Au-Fe | 668.5 | 439.5 | 418.5 |
| Cu-Fe | 441 | 388.5 | 538 |

** 1st peak had normalized height of 1, 2nd peak 0.75-0.4 and the 3rd peak 0.5-0.3.*

each corresponding wavelength. Each sample was measured a minimum of three times to establish reproducibility.

Fig. 3 shows the contribution of gold electrode to the emission spectra. Gold (24 carat) has a prominent emission at 669 nm that also shows up in the spectra of substances ionized by gold electrodes as discussed later. Table I summarizes prominent peaks we detected in gold and other common electrodes. Iron has a prominent emission at 440.5 nm. Copper has an emission spectrum that closely resembles gold with a prominent emission at 668.5 but has higher intensity at 418.5 nm and a lower intensity at 537.5 nm. Gold electrodes were selected for the experiment due to their ability to resist corrosion and material breakdown while having large voltages applied across them.

The electrode emission spectrum contributes to the emission spectra of other substances that we ionize to identify and should be accounted for. Another important substance present in most materials of interest is water and its emission spectrum ionized with gold electrodes is shown in Fig. 4. The water sample was prepared by using a micropipette to inject 30 microliters of distilled water into the sample holding vial. Gold's characteristic peak is still visible around the 669 nm

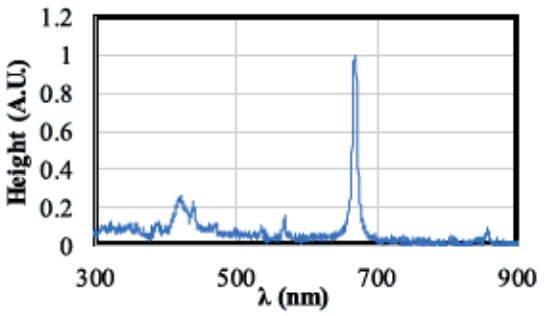


Fig. 4. Normalized plot of emission spectra contribution of water.

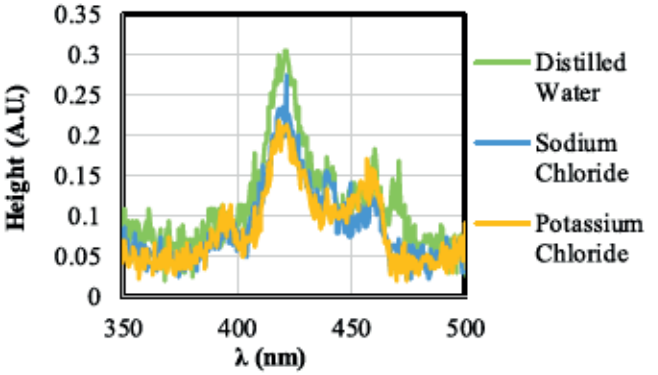


Fig. 5. Normalized plot of emission spectra of potassium chloride, sodium chloride, and water.

and the effect of the water can be seen in the 400-600 nm range.

Fig. 5 shows the emission spectrum of sodium chloride, potassium chloride, and sodium chloride all ionized with gold electrodes. The difference between the emission spectra of pure water, aqueous potassium chloride, and aqueous sodium chloride are quite clear. The water sample was prepared in the same manner as mentioned above. Both the aqueous sodium chloride and potassium chloride solutions were prepared by dissolving 0.05 g of each salt in 50 mL of water to create 10 percent potassium chloride and sodium chloride solutions. And as previously mentioned, 30 microliters of each solution were injected into the sample holder prior to ionization.

Viral particles are composed of surface proteins and deoxyribonucleic acid (DNA) or ribonucleic acid (RNA) genetic materials. In the process of ionization, the viral particles are fragmented to their different constituents followed by further fragmentations and their eventual molecular ionization. It is important to examine the possibility of detecting the ionization of these constituents through their emission spectra. Fig. 6 shows the emission spectra of the DNA bases adenine (A), guanine (G), cytosine (C) and thymine (T). In these experiments 1 $mm^3$ (~0.0025 g) of DNA bases powder were dissolved and ultrasonicated in 1 mL of water and the ionization cell was equipped with gold electrodes. The peak around 439 nm is due to the emission from the gold electrode that is slightly shifted by different amounts in the presence of different bases. Since the wavelength shifts differently, the spectral line can be used to identify the bases.

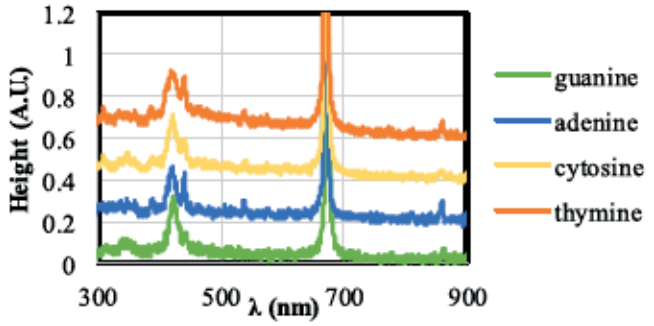


Fig. 6. Normalized plots of emission spectra of guanine, adenine, cytosine, and thymine solutions. Adenine, cytosine, and thymine plots were given an offset of +0.2, +0.4, and +0.6 respectively.

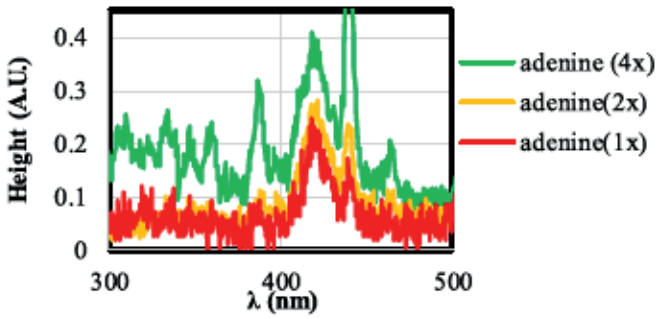


Fig. 7. Normalized emission spectra of adenine solutions with 0.0025g/mL (1×), 0.005g/mL (2×), and.01g/mL (4×) concentrations.

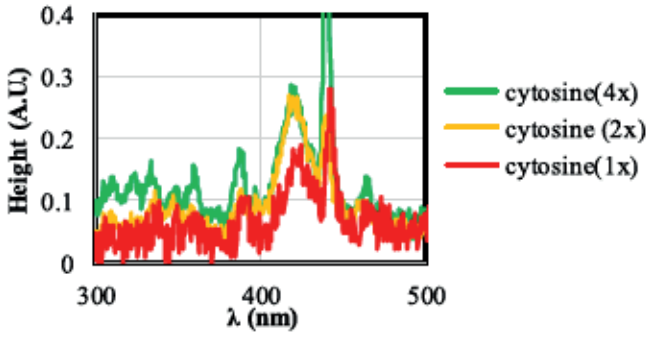


Fig. 8. Normalized plots of emission spectra of different concentrations 0.0025g/mL (1×), 0.005g/mL (2×), and 0.01g/mL (4×) of cytosine solutions.

Despite the DNA base concentrations being small in each solution, it is still possible to distinguish one solution from the other. The differences between each solution and gold's emission spectra are best seen in the 300 to 500 nm wavelength range. Figs. 7 and 8 show the differences between varying concentrations of adenine and cytosine. Each DNA base was prepared by adding the specified amount of DNA base powder to 1 mL of water, sonicating the mixture, and using a micropipette to inject 30 microliters of the solution into the sample holder prior to ionization.

Fig. 9 shows the peak emission values at 439.5 for adenine, 440 for cytosine, 440.5 for thymine, and 421.5 for guanine at different concentrations. Peak values were obtained by comparing data captured by the Oceanview spectrometer application to find the maximum height in the displayed window.

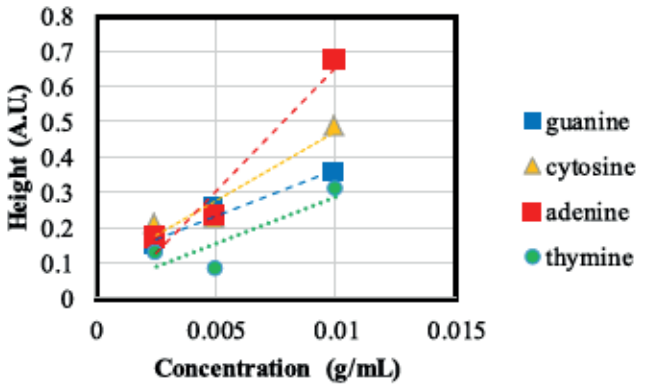


Fig. 9. Emission peaks at 439.5 for adenine, 440 for cytosine, 440.5 for thymine, and 421.5 for guanine as a function of their concentrations.

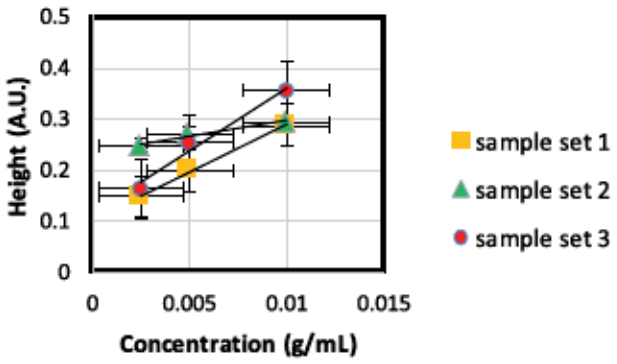


Fig. 10. Emission peaks for three different samples of guanine with error bars. Each sample set contained a sample with.0025 g/mL, .005g/mL, and.01 g/mL of guanine.

The average sensitivity was ~20%/g that was calculated by the change in the intensity of the emission line as substances were added to the solution. All the emission spectra were normalized to have maximum peak of 1 at the gold emission line. Thus, 20%/g is the change 0.2 per gram in the normalized scale.

There is a degree of variability between the emission spectrum of measurements taken on different days. These variations can be attributed to many things included noise, contaminants entering the sample holder, and slight variations in amounts of bases or materials being used to make different samples. However, these variations were not significant enough to be unable to recognize specific samples.

Fig. 10 shows the sensitivity plots of three different sets of guanine samples. Each set included a sample with the concentrations specified in Fig. 8.

Fig. 11 shows the emission spectra of fresh saliva in the same individual before and after a meal. One needs to account for important factors that contribute to saliva's emission spectrum to differentiate them from contributions of the viral particles. The individual was given a vial to collect a saliva sample with before a meal and a second and third vial for the two-time intervals after a meal. Experimenter wore gloves and a mask while preparing sample and cleaning area after each experiment. Each sample was prepared by using a micropipette to inject 30 microliters of the samples into the sample holder.

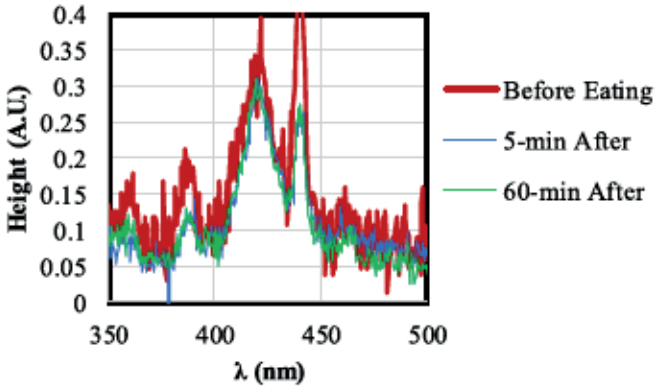


Fig. 11. Normalized emission spectra of fresh saliva before eating, five-minutes after eating, and within sixty-minutes of eating.

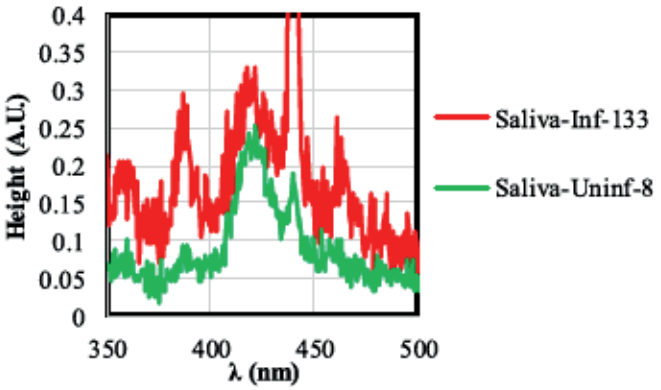


Fig. 12. Normalized emission spectra of uninfected and infected saliva.

The peak emission at 430 nm was considerably higher before a meal.

Fig. 12 shows the emission spectra of uninfected, and SARS-CoV-2 infected saliva. Fresh SARS-CoV-2 infected saliva were collected from patients in University Hospitals by our collaborator Dr. Elizabeth Middleton under study protocols approved by the Institutional Review Board of the University of Utah (IRB#: 00093575) and were transported to the sensor biosafety 2 laboratory in the engineering building. Uninfected salivae were collected from healthy tested students and other individuals. PCR was used to identify infected saliva. Typical viral load was around $10^6/\mu$L.

The emission spectrum of the uninfected saliva is similar to the emission spectrum shown in Fig. 10 of a different uninfected individual. Samples were carefully prepared by an experimenter wearing proper personal protection equipment and followed sanitary best practices while preparing and cleaning up after each experiment. For each sample 30 microliters of the saliva was injected into the sample holder using a micropipette prior to ionization. There are two peaks one at 425 nm and the other at 460 nm that are uniquely observed in the infected saliva.

Fig. 13 shows the reproducibility of these results by showing the peak values obtained at 460 nm and 425 nm for four different measurements of infected saliva.

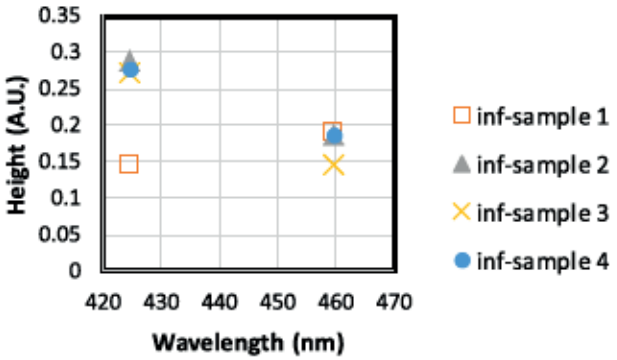


Fig. 13. Normalized peak values at 460 nm and 425 nm of different infected saliva measurements.

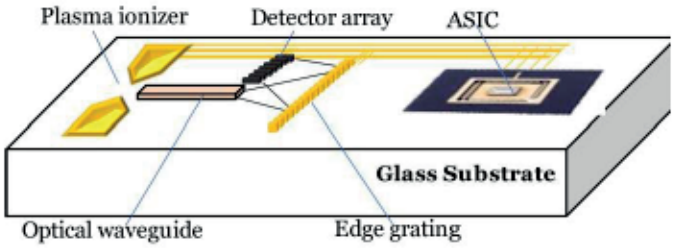


Fig. 14. Schematic of integrated plasma ionization spectroscopy microsystem for label-free detection of viral particles.

While one value for sample one obtained at 425 nm is significantly different than the other values, the other three samples stayed within a relatively tight range.

The above preliminary results demonstrate the possibility of using plasma ionization emission spectra to detect different substances. Clearly more work is needed to quantify the results and develop a theoretical framework for emission spectra of different substances in different environments.

It is important to note that the plasma ionization emission spectroscopy may be used to detect inactivated viral particles as well, but the wavelengths of emission lines will likely be different compared to the intact viruses. Inactivation of viruses is accomplished using heating, radiation, and strong oxidants/acids. Although the constituent parts of virus in these cases may remain in the vicinity of the inactivated virus, their ionization energies will likely to be different.

## IV. Device Miniaturization

The experimental setup (Fig. 1) used in our studies can be readily miniaturized. We have reported 1-100 $\mu$m microfabricated plasma devices in the past [13]–[15] that can also be used as ionization sources. The spectrometer can be miniaturized using MEMS approach as discussed in [16], [17]. Interference filters can also be implemented readily in waveguides [18] as well as in free space [19]. Optical detectors sensitive in the 300 nm to 900 nm can be realized with silicon and are well established [19]. Fig. 14 shows the schematic of a miniaturized plasma ionization sensor that is being developed by the authors. Most of the studies and experimental results presented here are preliminary and can be viewed as feasibility studies. However, the ability to produce a miniature plasma

ionization emission spectroscopy device to detect viral particles and chemicals will enable field-operable point-of-care sensors and devices urgently needed in controlling the spread of SARS-CoV-2 pandemic.

## V. Conclusion

We demonstrated the application of plasma ionization technique to detect different substances from the aqueous phase including DNA bases and SARS-CoV-2 infected saliva. The technique is label free and can be miniaturized for wide range of applications.

## Acknowledgment

Infected salivae were obtained from Dr. Elizabeth Middleton of the Department of Internal Medicine, The University of Utah. SARS-CoV-2 sensors partially discussed here are being commercialized by The University of Utah. Please contact Dr. Aaron Duffy (aaron.duffy@utah.edu) for more information.

## References

[1] H. Muto *et al.*, "Plasma spectroscopy of metal ions for hyper-electron cyclotron resonance ion source," *Rev. Sci. Instrum.*, vol. 85, no. 2, Feb. 2014, Art. no. 02A905, doi: 10.1063/1.4825160.

[2] H. Muto *et al.*, "Grating monochromator for electron cyclotron resonance ion source operation," *Rev. Sci. Instrum.*, vol. 84, no. 7, 2013, Art. no. 073304, doi: 10.1063/1.4813078.

[3] I. G. McWilliam and R. A. Dewar, "Flame ionization detector for gas chromatography," *Nature*, vol. 181, p. 760, Mar. 1958, doi: 10.1038/181760a0.

[4] W. M. Holber, "Ionization by microwave electron cyclotron resonance plasma," in *Thin Films*, vol. 27, J. A. Hopwood, Ed. Amsterdam, The Netherlands: Elsevier, 2000, pp. 67–94, doi: 10.1016/S1079-4050(00)80006-X.

[5] M. Haschke, *Laboratory Micro-X-Ray Fluorescence Spectroscopy*. Cham, Switzerland: Springer, 2014.

[6] H. B. Steen, O. I. Sørensen, and J. A. Holteng, "Observation of X-ray- and U.V.-induced luminescence and absorption during and after the irradiation," *Int. J. Radiat. Phys. Chem.*, vol. 4, no. 1, pp. 75–86, 1972, doi: 10.1016/0020-7055(72)90010-1.

[7] N. Yamamoto, K. Araya, and F. J. de Abajo, "Photon emission from silver particles induced by a high-energy electron beam," *Phys. Rev. B, Condens. Matter*, vol. 64, Nov. 2001, Art. no. 205419.

[8] J. T. Gudmundsson and A. Hecimovic, "Foundations of DC plasma sources," *Plasma Sources Sci. Technol.*, vol. 26, no. 12, 2017, Art. no. 123001.

[9] H. Tao, T. Nakazato, M. Akasaka, and S. Satoh, "Speciation of sulfur in petroleum liquids by gas chromatography/inductively coupled plasma mass spectrometry," *Bunseki Kagaku*, vol. 56, no. 5, pp. 333–347, 2007, doi: 10.2116/bunsekikagaku.56.333.

[10] J. Hyun, S.-G. Lee, and J. Hwang, "Application of corona discharge-generated air ions for filtration of aerosolized virus and inactivation of filtered virus," *J. Aerosol Sci.*, vol. 107, pp. 31–40, May 2017, doi: 10.1016/j.jaerosci.2017.02.004.

[11] M. Hagbom, J. Nordgren, R. Nybom, K.-O. Hedlund, H. Wigzell, and L. Svensson, "Ionizing air affects influenza virus infectivity and prevents airborne-transmission," *Sci. Rep.*, vol. 5, no. 1, p. 11431, Sep. 2015, doi: 10.1038/srep11431.

[12] M. Tabib-Azar and P. Pai, "Microplasma field effect transistors," *Micromachines*, vol. 8, no. 4, p. 117, 2017.

[13] P. Pai and M. Tabib-Azar, "Micro-plasma field effect transistor operating with DC plasma," *IEEE Electron Device Lett.*, vol. 35, no. 5, pp. 593–595, May 2014.

[14] P. Pai and M. Tabib-Azar, "Microplasma logic gates," *IEEE Trans. Plasma Sci.*, vol. 42, no. 8, pp. 1995–1998, Aug. 2014.

[15] M. Tabib-Azar, *Integrated Optics and Microstructure Sensors*. Boston, MA, USA: Kluwer, 1995.

[16] G. Zhou, Z. H. Lim, Y. Qi, F. S. Chau, and G. Zhou, "MEMS gratings and their applications," *Int. J. Optomechtron.*, vol. 15, no. 1, pp. 61–86, Jan. 2021, doi: 10.1080/15599612.2021.1892248.

[17] K. Knop, H. W. Lehmann, and R. Widmer, "Microfabrication and evaluation of diffractive optical filters prepared by reactive sputter etching," *J. Appl. Phys.*, vol. 50, no. 6, pp. 3841–3848, Jun. 1979, doi: 10.1063/1.326499.

[18] T. Ngernsutivorakul *et al.*, "Design and microfabrication of a miniature fiber optic probe with integrated lenses and mirrors for Raman and fluorescence measurements," *Anal. Bioanal. Chem.*, vol. 409, no. 1, pp. 275–285, Jan. 2017, doi: 10.1007/s00216-016-9999-5.

[19] A. Sosna-Głębska, M. Sibiński, N. Szczecińska, and A. Apostoluk, "UV–visible silicon detectors with zinc oxide nanoparticles acting as wavelength shifters," *Mater. Today: Proc.*, vol. 20, pp. 25–29, Sep. 2020, doi: 10.1016/j.matpr.2019.08.157.

**Massood Tabib-Azar** (Senior Member, IEEE) received the M.S. and Ph.D. degrees in electrical engineering from the Rensselaer Polytechnic Institute in 1984 and 1986, respectively.

In 1987, he joined the Faculty of the EECS Department, Case Western Reserve University. He was a Fellow at NASA from 1992 to 1992, on sabbatical at Harvard University from 1993 to 1994, at Yale University from 2000 to 2001, at UC Berkeley from 2015 to 2016, and at the Massachusetts Institute of Technology in 2016. He was the Program Director at the ECCS Division of National Science Foundation from 2012 to 2013. He is currently a USTAR Professor of ECE at the Electrical and Computer Engineering Department, The University of Utah, with an adjunct appointment at the Bioengineering Department. He is an author of three books, two book chapters, more than 270 journal publications, and numerous conferences proceeding articles. His current research interests include nanometrology, micro-plasma devices, nano-electromechanical computers, novel devices based on solid electrolytes (memristors), sensors and actuators, injectable bio-systems, quantum sensing, and quantum computing. His teaching interests include development of courses in electronic device physics and electromagnetics with an emphasis on solving problems and the use of computer-aided instruction tools. He has introduced and chairs many international symposia in his fields of interest. He is a member of the New York Academy of Sciences, APS, AAPT, and Sigma Xi research societies. He is in the Editorial Board of IEEE ELECTRON DEVICE LETTERS. Dr. Tabib-Azar was a recipient of the 1991 Lilly Foundation Fellowship. He has received more than 14 certificate of appreciation and recognition for his professional activities and the Best Paper Award from Design Automation Conference in 2001 for his work on electromagnetic properties of interconnects and defects in ICs, the Best Paper Award from the International Conference on Intelligent Robots and Systems in 2004 for his work on human–machine interface, and the Best Paper Award from ISQED for his work on NEMS Processors in 2011.

**Braden Aaron Brown** is pursuing the B.S. and M.S. degrees in electrical engineering with The University of Utah, as part of the College of Engineering's Combined M.S./B.S. Program. His study interests include device physics, wireless communications, and medical devices. His other areas of research involve focused ultrasound (FUS) treatments of epilepsy.